

Seeing through multimode fibers with real-valued intensity transmission matrices

Tianrui Zhao, Sebastien Ourselin, Tom Vercauteren, Wenfeng Xia*

School of Biomedical Engineering and Imaging Sciences, King's College London, 4th Floor, Lambeth

Wing St Thomas' Hospital London, London SE1 7EH, United Kingdom

*Corresponding author: *wenfeng.xia@kcl.ac.uk

Abstract

Image transmission through multimode optical fibers has been an area of immense interests driven by the demand for miniature endoscopes in biomedicine and higher speed and capacity in telecommunications. Conventionally, a complex-valued transmission matrix is obtained experimentally to link the input and output light fields of a multimode fiber for image retrieval, which complicates the experimental setup and increases the computational complexity. Here, we report a simple and high-speed method for image retrieval based on our discovery of a pseudo-linearity between the input and output light intensity distributions of multimode fibers. We studied the impact of several key parameters to image retrieval, including image pixel count, fiber core diameter and numerical aperture. We further demonstrated that a wide variety of input binary images could be faithfully retrieved from measured output speckle patterns using this method, promising to be useful for highly miniaturized endoscopy in biomedicine and spatial-mode-division multiplexing in telecommunications.

Introduction

Multimode optical fibers (MMFs) have been increasingly attractive for applications in biomedical endoscopy and telecommunications, owing to the capability of transporting light via a large number of transverse optical modes. For biomedical endoscopy, the number of transverse modes in an MMF represents the number of pixels in the images. Compared to multi-core coherent fiber bundles that are commonly used in biomedical endoscopy, MMFs are significantly more cost-effective, and the effective pixel density in an MMF can be 1-2 orders of magnitudes greater [1-2]. For telecommunications, MMFs are attractive due to the potential of multiplexing data within the large number of modes. However, light propagation in MMFs suffers from modal dispersion and mode coupling; For example, when projecting an image pattern onto the proximal fiber tip, the light couples into different modes with different propagation constants and thus forms a random-like speckle pattern at the distal end [1,3,4]. Therefore, the propagation characteristics of an MMF are required for faithfully retrieving input patterns from measured speckle patterns.

Wavefront shaping has been an emerging technology for controlling light transport in disordered media [5-16]. A number of research groups [7-11] have studied the transmission matrix (TM) theory for image transmission through disordered media such as MMFs. In this theory, the disordered medium is characterized by a complex-valued matrix, which connects the input and output light fields with complex-valued transmission constants that represent the changes of light field during the light transport [6,8-11]. Therefore, the input light field can be calculated when the TM and the output light field (phase and amplitude) are known. However, conventional cameras are only able to capture the light intensity, and the phase

information is usually obtained using holographical methods with a complex optical reference arm that can degrade the system stability [8-11].

Recently, image retrievals through disordered media using only the intensity information of the output light field were achieved with deep learning [17-21] and model-based methods [22], allowing a simpler optical system compared to those of TM-based methods. With deep learning, a large set of input-output image pairs were used to train a multi-layer neural network for predicting input images such as handwritten digits [17] and letters [19], and Quickdraw objects [18]. However, the requirements for large datasets and iterative optimization processes resulted in prolonged time for data acquisition and neural network training. Further, the performance of the trained neural network is likely to depend on similarities between the testing and training datasets. Most recently, a model-based method was used to characterize an MMF [22]. With this method, a set of input images were projected onto one end of an MMF whilst the intensity values of the outputs at the other end were converted into amplitude (square root of the intensity) information with zero phase. With these input-output pairs, an iterative algorithm was used to obtain a complex-valued matrix as the inverse TM of the fiber. Different from the deep learning methods, this matrix explicitly linked the input images with the output speckles with a physically-informed model and hence allowed the retrieval of images of complex natural scenes [22]. However, large datasets and time-consuming iterative optimization were required for calculating the complex-valued matrix, which limited its applicability. Thus, a simple and high-speed approach to characterize MMFs is highly desired.

In this work, we developed, for the first time to the best of our knowledge, a method to characterize an MMF with a real-valued intensity transmission matrix (ITM), which connects the input and output light intensities and hence to retrieve input images from the intensity values of the output speckles. This method is based on our discovery of a pseudo-linearity between the input and output intensity distributions of MMFs. Importantly, as calculating real-valued ITMs was achieved without a time-consuming iterative process or a large database, this method allowed a high-speed characterization to be performed within \sim 16 s (\sim 8.2 s for data acquisition and \sim 7.8 s for ITM calculation) for retrieving images with 1024 pixels and hence paved the way for the practical uses of MMFs in endoscopy and telecommunications applications.

Results

A number of experiments were performed to investigate the impact of several key parameters to the performance of image retrieval. The relationship between the switched ‘ON’ pixel count of input images (J) to the pseudo-linearity is shown in Fig. 1. With a constant input pixel count (1024), the correlation coefficient, indicating the fidelity of image retrieval, increased rapidly from \sim 5% to \sim 90% with J increasing from 32 to 384, and remained largely consistent with J in the range of 384 to 896. With J increasing from 896 to 1024, the correlation coefficient declined rapidly, which can be attributed to the loss of low spatial frequency components due to the diffraction of the DMD micromirrors. This suggests that the pseudo-linearity is dependent on the J values. One possible explanation is that as the input binary patterns for characterization had 50% pixels with “1” value, the resulting ITM was more suitable for retrieving input images with a similar intensity distribution as those used in

characterization. However, further investigations are required to better understand this dependency.

The impact of total input pixel count (N) is shown in Fig. 2. With the same input image pattern, the input images with more pixels had lower correlation coefficients. The fiber core diameter and numerical aperture (NA) also had significant impact on the retrieved image quality, which could be attributed to the impact of the number of supported transverse modes in the MMFs. MMFs with larger numbers of supported transverse modes were able to transmit images with larger input pixel counts. More examples of retrieved images with different input pixel counts and MMFs can be found in Fig. S1 (Supplement 1). The computation time for ITM estimation increased with both the input and output pixel counts (N and M). For example, with a desktop PC (Intel i7 8700, 3.2 GHz), when N and M increased from 32×32 and 360×360 to 64×64 and 500×500, the computation time for ITM estimation, and image reconstruction increased from ~8 s to ~240 s, and 0.01 s to 0.05 s, respectively. In contrast, the computation time for fiber characterization with deep learning- and model-based methods can be several hours [18]. To achieve a greater pixel count while maintaining good fidelity, MMFs with larger core diameters and/or numerical apertures could be used as they support larger numbers of transverse modes. However, it is notable that this will result in increased computational time for fiber characterization and image reconstruction, which could be mitigated with parallel computing.

The impact of the variability of input image patterns is show in Fig. 3. The fidelity of the retrieved images was weakly dependent on the input patterns: correlation coefficients varied from 91.76% for a handwritten digit to 97.62% for a random binary pattern. After binarization,

correlation coefficients for all the types of input images increased and were greater than 99% in most of the cases. With a higher number of input pixels (64×64), the correlation coefficient varied from 74.84% for the handwritten digit to 90.91% for the random binary pattern, respectively (see Supplement 1 Fig. S2). Two videos showing retrieved images from a series of output speckles through the same fiber are shown in Visualizations 1, 2.

Discussion and conclusions

Compared with other existing methods, our approach has a number of distinct advantages. First, the fiber characterization process with our method requires both a short time for calculation and data acquisition. In contrast, both the training process of deep learning-based methods and model-based algorithms rely on iterative optimization that is usually very time-consuming (several hours). Furthermore, they require large training datasets and hence a relatively long data acquisition time. This is problematic when repeated fiber characterization process is required due to speckle decorrelations. Second, the retrieved image quality with our method is weakly dependent on the types of input images. However, deep learning-based approaches are most likely to work only for images that are similar to the training datasets [17-21]. Last, the experimental setup is much simpler compared to those of holographical methods with complex optical reference arms that can degrade the stability of the system.

Similar to other methods, our method also suffers from speckle decorrelations induced by fiber deformations. One mitigation solution could be to integrate an MMF within a rigid medical catheter or needle for biomedical applications. Recently, it was reported that with the knowledge of the fiber shape, TM of the fiber can be corrected to compensate

deformations-induced speckle decorrelations [1]. A similar approach could be used in the future to correct for the deformation-induced changes in ITM for image retrieval.

In conclusion, we developed a method to measure the light intensity transmission characteristics for an MMF with a real-valued ITM, and with this, input light intensity distributions can be reconstructed from the measured output light intensity distributions. This method enables a high-speed MMF characterization, and high-fidelity image retrievals using a simple measurement setup, and thus could be useful for several applications in biomedical endoscopy and telecommunications.

REFERENCES

1. Plöschner, M. Tyc, T. & Čižmár, T. Seeing through chaos in multimode fibers. *Nat. Photonics* 9, 529–535 (2015).
2. Andresen, E. R. Sivankutty, S. Tsvirkun, V. Bouwmans, G. & Rigneault, H. Ultrathin endoscopes based on multicore fibers and adaptive optics: a status review and perspectives. *J. Biomed. Opt.* 21, 121506–121506 (2016).
3. Xiong, W. Hsu, C. & Cao, H. Long-range spatio-temporal correlations in multimode fibers for pulse delivery. *Nat. Commun.* 10, 1-7 (2019).
4. Xiong, W. Ambichl, P. Bromberg, Y. Redding, B. Rotter, S. & Cao, H. Principal modes in multimode fibers: exploring the crossover from weak to strong mode coupling. *Opt. Express* 25, 2709–2724 (2017).
5. Vellekoop, I. & Mosk, A. Focusing coherent light through opaque strongly scattering media. *Opt. Lett.* 32, 2309–2311 (2007).

6. Mosk, A. P. Lagendijk, A. Lerosey, G. & Fink, M. Controlling waves in space and time for imaging and focusing in complex media. *Nat. Photonics* 6, 283–292 (2012).
7. Popoff, S. Lerosey, G. Carminati, R. Fink, M. Boccara, A. & Gigan, S. Measuring the transmission matrix in optics: an approach to the study and control of light propagation in disordered media. *Phys. Rev. Lett.* 104, 100601 (2010).
8. Čižmár, T. & Dholakia, K. Shaping the light transmission through a multimode optical fiber: complex transformation analysis and applications in biophotonics. *Opt. Express* 19, 18871–18884 (2011).
9. Cižmár, T. & Dholakia, K. Exploiting multimode waveguides for pure fiber-based imaging. *Nat. Commun.* 3, 1027 (2012).
10. Loterie, D. Farahi, S. Papadopoulos, I. Goy, A. Psaltis, D. & Moser, C. Digital confocal microscopy through a multimode fiber. *Opt. Express* 23, 23845–23858 (2015).
11. Choi, Y. Yoon, C. Kim, M. Yang, T. D. Fang-Yen, C. Dasari, R. R. Lee, K. J. & Choi, W. Scanner-free and wide-field endoscopic imaging by using a single multimode optical fiber. *Phys. Rev. Lett.* 109, 203901 (2012).
12. Wang, D. Zhou, E. H. Brake, J. Ruan, H. Jang, M. & Yang, C. Focusing through dynamic tissue with millisecond digital optical phase conjugation. *Optica* 2, 728–735 (2015).
13. Lai, P. Wang, L. Tay, J. W. & Wang, L. V. Photoacoustically guided wavefront shaping for enhanced optical focusing in scattering media. *Nat. Photonics* 9, 126–132 (2015).
14. Katz, O. Small, E. Bromberg, Y. & Silberberg, Y. Focusing and compression of ultrashort pulses through scattering media. *Nat. Photonics* 5, 372–377 (2011).
15. Conkey, D. B. Caravaca-Aguirre, A. M. & Piestun, R. High-speed scattering medium characterization with application to focusing light through turbid media. *Opt. Express* 20, 1733–1740 (2012).

16. Leonardo, R. Di & Bianchi, S. Hologram transmission through multi-mode optical fibers. *Opt. Express* 19, 247–254 (2011).
17. Borhani, N. Kakkava, E. Moser, C. & Psaltis, D. Learning to see through multimode fibers. *Optica* 5, 960-966 (2018).
18. Rahmani, B. Loterie, D. Konstantinou, G. Psaltis, D. & Moser, C. Multimode optical fiber transmission with a deep learning network. *Light Sci. Appl.* 7, 69 (2018).
19. Li, Y. Xue, Y. & Tian, L. Deep speckle correlation: a deep learning approach towards callable imaging through scattering media. *Optica* 5, 1181–1190 (2018).
20. Turpin, A. Vishniakou, I. & Seelig, J. d. Light scattering control in transmission and reflection with neural networks. *Opt. Express* 26, 30911–30929 (2018).
21. Li, S. Deng, M. Lee, J. Sinha, A. & Barbastathis, G. Imaging through glass diffusers using densely connected convolutional networks. *Optica* 5, 803–813 (2018).
22. Caramazza, P. Moran, O. Murray-Smith, R. & Faccio, D. Transmission of natural scene images through a multimode fiber. *Nat. Commun.* 10, 2029 (2019).
23. Edgar, M. P. Gibson, G. M. & Padgett, M. J. Principles and prospects for single-pixel imaging. *Nat. Photonics* 13, 13–20 (2019).

Methods

Experimental setup

The intensity of a light beam from a pulsed laser (532 nm, 2 ns, SPOT-10-200-532, Elforlight, Daventry, United Kingdom) was spatially modulated using a DMD (DLP7000, 768×1080 pixels, Texas Instruments, Texas, USA) with a set of binary patterns, and then projected onto the proximal end of a MMF (\varnothing 200 μ m, 0.22 NA, 1 m, M122L01, Thorlabs, New Jersey, USA) via a tube lens (AC254-050-A-ML, Thorlabs, New Jersey, USA) and an objective (20 \times , 0.4 NA,

RMS20X, Thorlabs, New Jersey, USA). After magnification with an objective (20 \times , 0.4 NA, RMS20X, Thorlabs, New Jersey, USA) and a tube lens (AC254-0100-A-ML, Thorlabs, New Jersey, USA), the intensities of the output speckles at the other end were captured by a CMOS camera (C11440-22CU01, Hamamatsu Photonics, Shizuoka, Japan) and used for fiber characterization and image retrieval.

Image retrieval with a real-valued intensity transmission matrix

Image retrieval via a real-valued ITM required a characterization step and a subsequent image reconstruction step as illustrated in Fig 4. In the characterization step, Hadamard matrices, which have been widely used in compressive sensing technologies [23], were used to construct the binary patterns for characterization. A Hadamard matrix $H \in (-1, +1)$ with a size of N by N , was converted into two binary matrices H_1 and H_2 via the formulas $H_1 = (H+1)/2$, and $H_2 = (-H+1)/2$, respectively. Each column of a binary matrix $[H_1, H_2]$ was then converted to a square matrix ($\sqrt{N} \times \sqrt{N}$) and used as a binary pattern on the DMD, resulting in a total number of $2N$ binary Hadamard patterns as inputs. Here we defined an ITM that connected the intensities of the input patterns and the output speckles as:

$$\begin{bmatrix} I_1^1 & \dots & I_1^p \\ \vdots & \ddots & \vdots \\ I_m^1 & \dots & I_m^p \end{bmatrix} = ITM * [H_1, H_2] \quad (1)$$

where I_m^p represented the intensity value at the m^{th} pixel in the p^{th} output speckle, and each column of this matrix represented a vectorized input pattern. As all micromirrors were switched ‘ON’ in the first binary Hadamard pattern, Equation. 2 was further expressed to arrive at a Hadamard matrix $[H, -H] \in (-1, +1)$ on the right-hand side as:

$$\begin{bmatrix} 2I_1^1 - I_1^1 & \dots & 2I_1^p - I_1^1 \\ \vdots & \ddots & \vdots \\ 2I_m^1 - I_m^1 & \dots & 2I_m^p - I_m^1 \end{bmatrix} = ITM * [2H_1 - 1, 2H_2 - 1] = ITM * [H, -H] \quad (2)$$

so that the **ITM** can be obtained as:

$$ITM = \begin{bmatrix} 2I_1^1 - I_1^1 & \dots & 2I_1^p - I_1^1 \\ \vdots & \ddots & \vdots \\ 2I_m^1 - I_m^1 & \dots & 2I_m^p - I_m^1 \end{bmatrix} * [H, -H]^T \quad (3)$$

where $[H, -H]^T$ is the transpose of $[H, -H]$, and $[H, -H]^T = [H, -H] - 1$.

In the second step, the **ITM** was used to reconstruct input images from the output speckles using linear inversion as:

$$I_{image} = ITM^{-1} * I_{out} \approx I_{in} \quad (4)$$

where I_{image} is the intensity distribution of the retrieved input pattern, I_{out} is the intensity distribution of output speckle measured by the camera at the distal fiber tip, I_{in} is the intensity distribution of the ground truth. Here we define this approximate linear relationship between the input and output intensities as a pseudo-linearity.

Experiments

To study the relationship between the intensity distribution of the input image to the pseudo-linearity, the number of switched ‘ON’ pixel (J) was varied from 32 to 1024 while the total number of input pixels remained constant (1024) using an MMF ($\phi 200 \mu\text{m}$, 0.22 NA, 1 m, 9304 modes). With each J , 64 different input patterns were generated by switching ‘ON’ the micromirrors at J random positions.

To study the impact of total pixel count of the input patterns (N), the size of the binary patterns for characterization was varied from 8×8 , 16×16 , 32×32 to 64×64 , producing ITMs with varying input pixel counts. The number of illuminated micromirrors on the DMD was

kept constant (64×64 micromirrors), while different numbers of micromirrors were defined as one pixel to change the input pixel count. After characterization, a set of binary random patterns (with approximately half of the micromirrors were ‘ON’) were projected onto the DMD as the input ground truths. As such, although the same set of input patterns were used, the pixel counts of the ground truths and the retrieved images were varied with N.

To study the impact of the number of supported transverse modes of a MMF, three MMFs with different core diameters and NA were tested ($\varnothing 105 \mu\text{m}$, NA=0.22, length = 1 m, number of modes = 9304; $\varnothing 200 \mu\text{m}$, NA=0.22, length = 1 m, number of modes = 33756; $\varnothing 200 \mu\text{m}$, NA=0.50, length = 1 m, number of modes = 174360).

To demonstrate the impact of the variability of input images, binary images of different types, including handwritten digits (from MNIST database), schematic plants, animals, Chinese characters and random patterns, were studied for image retrievals through a step-index multimode fiber ($\varnothing 200 \mu\text{m}$, NA=0.22, length = 1 m). In addition, the retrieved images were further binarized using thresholds determined based on their histograms.

Acknowledgements

This work was supported by the Wellcome Trust [203148/Z/16/Z; WT101957] and the Engineering and Physical Sciences Research Council (EPSRC) [NS/A000049/1; NS/A000027/1]. T.V. is supported by a Medtronic / Royal Academy of Engineering Research Chair [RCSR1819\7\34].

Contributions

T.Z. and W.X. conceived of and performed the study, and wrote the paper. W.X. and T.V. supervised the project. S.O. provided scientific mentorship throughout the project. All the authors discussed the results and commented on the manuscript.

Competing Interests

The authors declare that there are no conflicts of interest. T.V. holds shares from Mauna Kea Technologies, Paris, France, which, however, did not support this work.

Data availability

The data and scripts that support the findings of this study are available from the corresponding author on reasonable request.

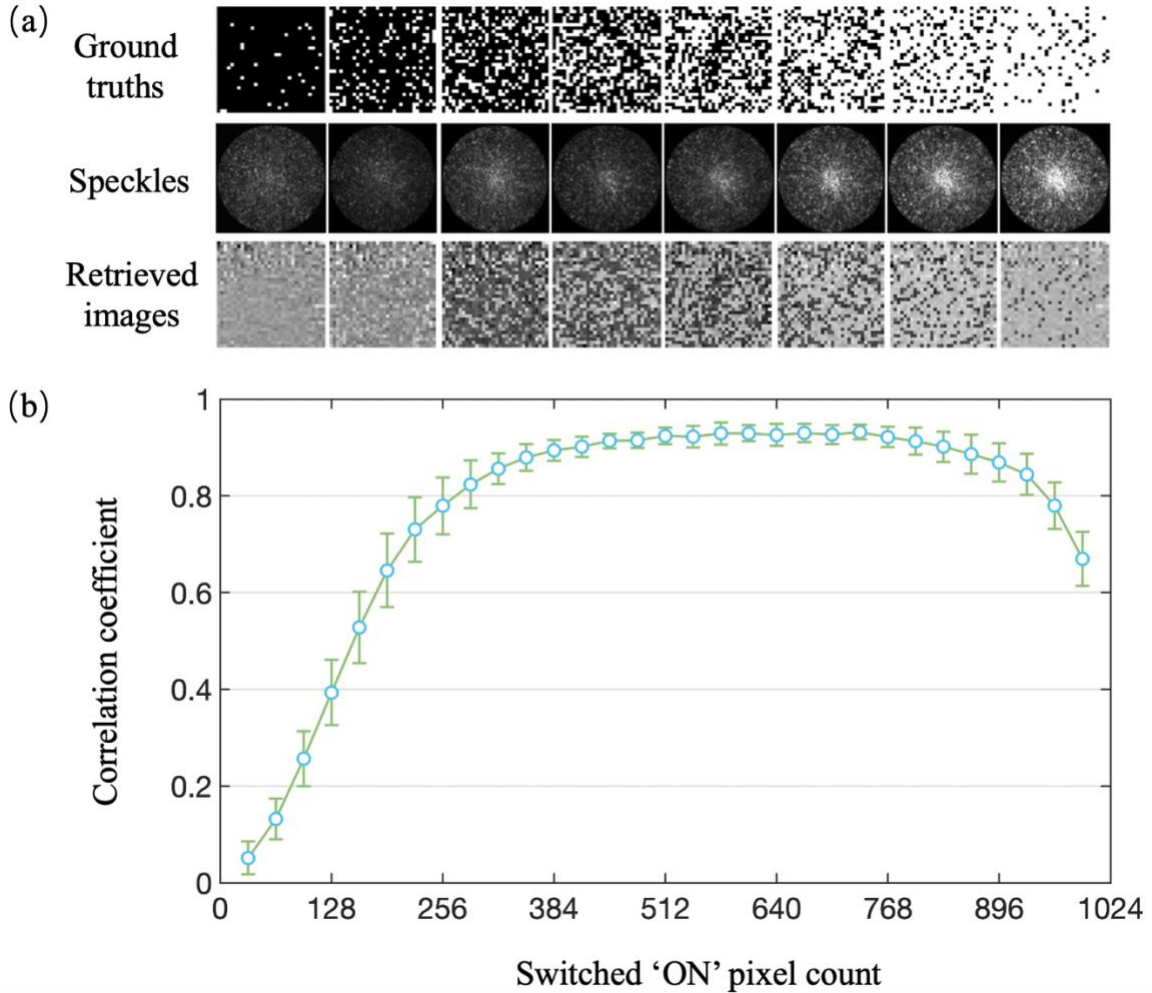


Fig. 1. Impact of switched 'ON' pixel count. (a) Some examples of image retrievals with varying switched 'ON' pixels count from 32 to 928 (left to right). (b) Correlation coefficients between the retrieved images and their ground truths as a function of the switched 'ON' pixels count. Data represent average values across 64 input patterns with the same J , and error bars represent standard deviations.

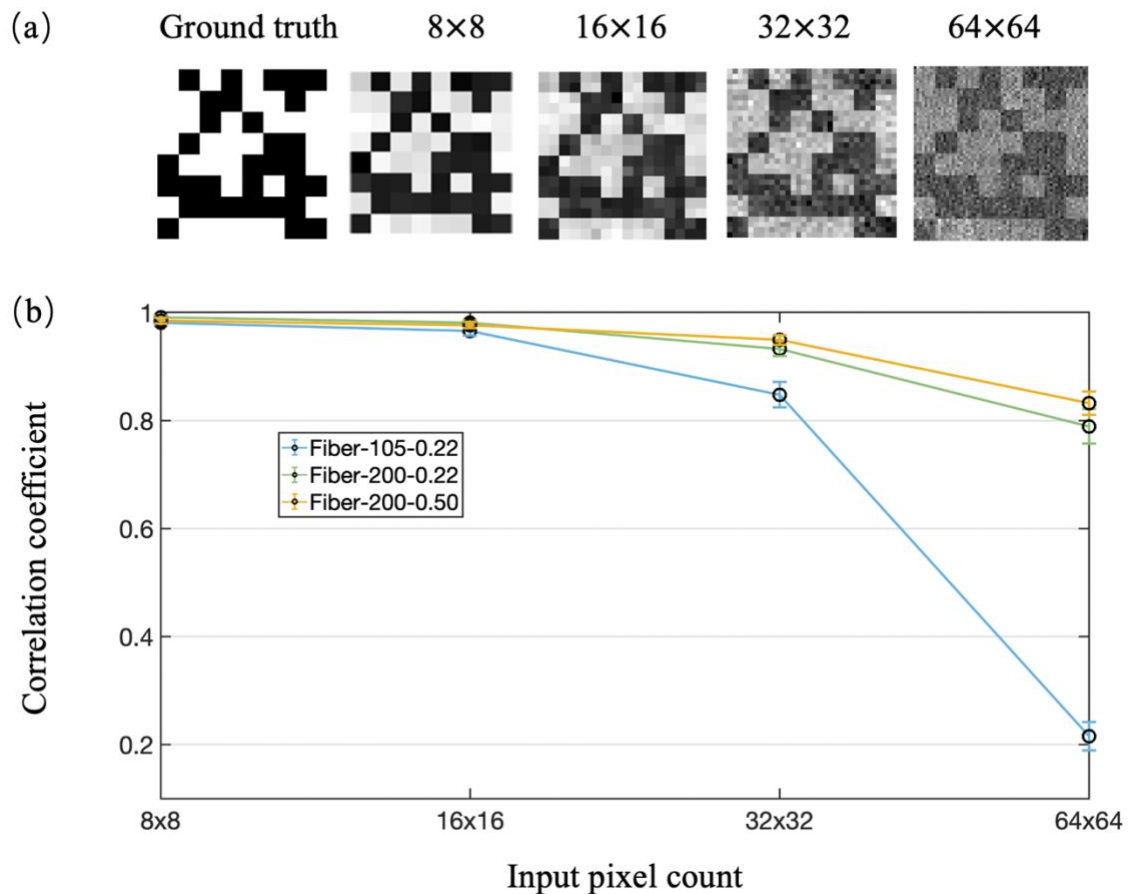


Fig. 2. Impact of input pixel count and number of supported transverse modes in multimode fibers (MMFs). (a) Retrieved images with the same ground truth and different input pixel counts through an MMF with a core diameter of 200 μm and a numerical aperture of 0.22. Retrieved images with the same ground truth and the other two MMFs can be found in Fig. S2 (Supplement 1). (b) Evolution of image retrieval performance with different MMFs and input pixel counts. Data represent average values across 64 input patterns with the same input pixel count, and error bars represent standard deviations. Fiber-105-0.22, $\varnothing 105 \mu\text{m}$, NA=0.22, length = 1 m; Fiber-200-0.22, $\varnothing 200 \mu\text{m}$, NA=0.22, length = 1 m; Fiber-200-0.50, $\varnothing 200 \mu\text{m}$, NA=0.50, length = 1 m.

Ground truths							
Speckles							
Retrieved images							
Correlation coefficient	91.76%	93.96%	95.20%	96.51%	95.25%	94.34%	94.05%
Binarized retrieved images							
Correlation coefficient	97.12%	99.54%	100%	99.74%	99.61%	100%	99.39%

Fig. 3. Image retrievals with different types of input patterns. Retrieved images were obtained from a step-index multimode fiber with a diameter of 200 μm , and numerical aperture of 0.22, and compared to their ground truths. The input pixel count was 32 \times 32. Examples with an input pixel count of 64 \times 64 shown in Fig. S1 (Supplement 1) and visualizations 1 and 2. More examples can be found in Fig. S3-S6, Supplement 1.

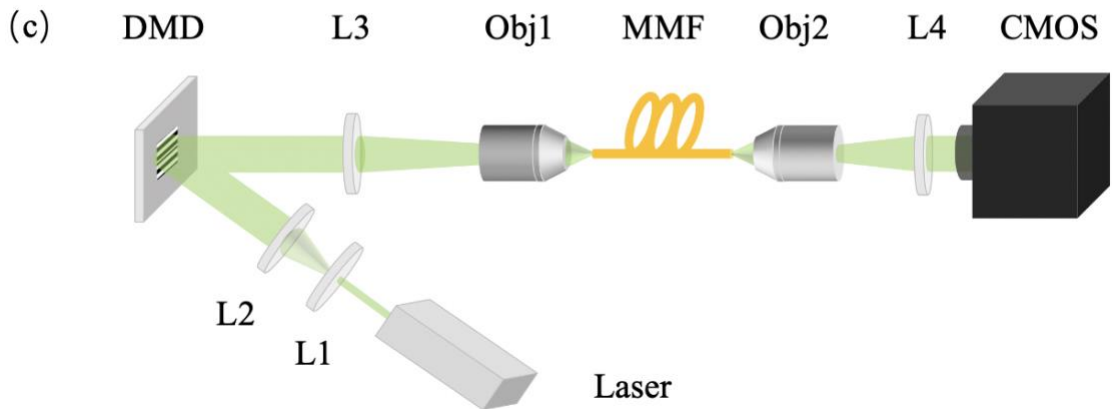
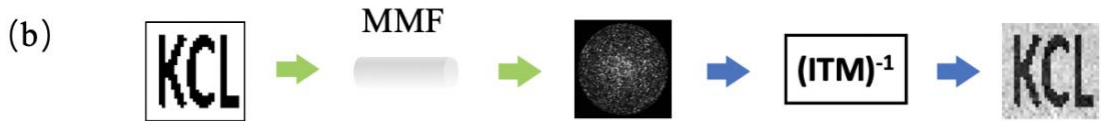
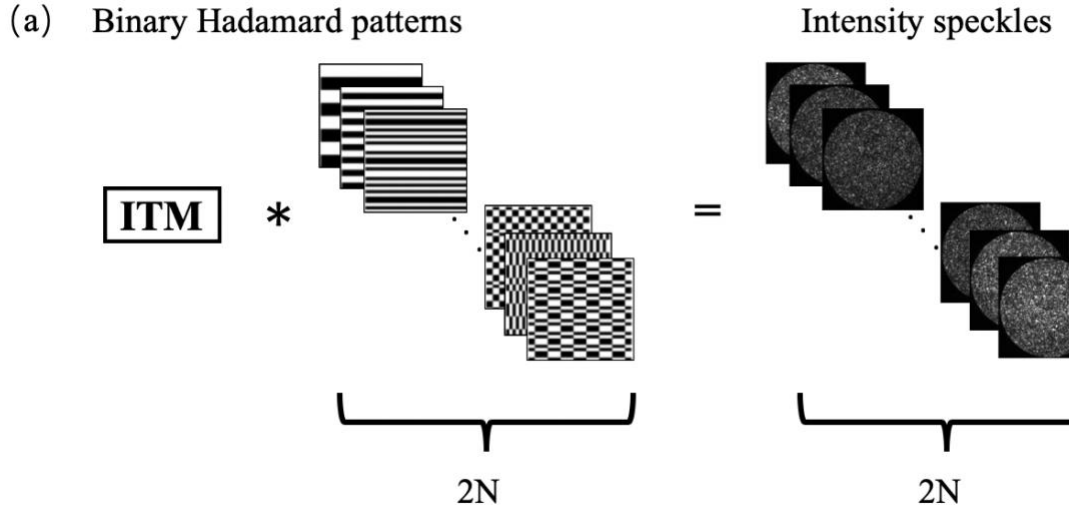


Fig. 4. Schematic illustrations of the principle and experimental setup of image retrieval through a multimode fiber with a real-valued intensity transmission matrix (ITM). (a) The method of multimode fiber characterization with ITM. To obtain the ITM, a set of binary Hadamard patterns are projected onto the proximal end of a multimode fiber with a DMD, whilst intensity values of the speckles at the other end are captured by a camera. (b) The process of retrieving an input image pattern (letters 'KCL') from the corresponding speckle pattern with the calculated ITM. (c) Schematic diagram of the experimental setup. L1-L4, tube lens; Obj1-Obj2, 20 \times objectives; DMD, digital micromirrors device; MMF, multimode fiber; CMOS, camera.

Seeing through multimode fibers with real-valued intensity transmission matrices

Tianrui Zhao, Sebastien Ourselin, Tom Vercauteren, Wenfeng Xia*

School of Biomedical Engineering and Imaging Sciences, King's College London, 4th Floor, Lambeth

Wing St Thomas' Hospital London, London SE1 7EH, United Kingdom

*Corresponding author: *wenfeng.xia@kcl.ac.uk

This document provides supplementary information to “Seeing through multimode fibers with real-valued intensity transmission matrix”. It includes more examples of image retrievals through different multimode fibers, and with different input patterns.

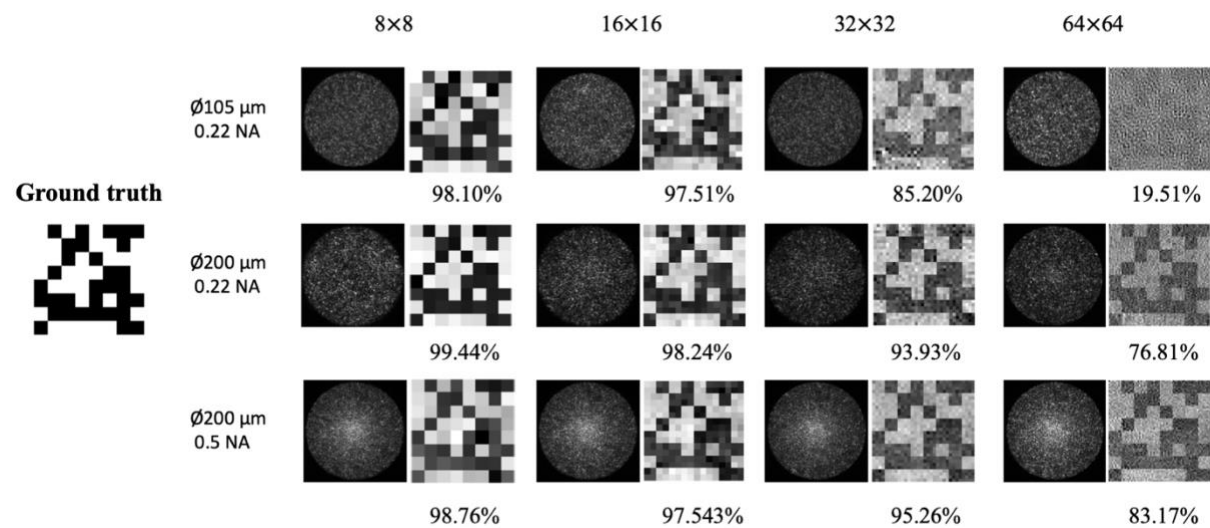


Fig. S1. The results of image retrievals through three different fibers with the same ground truth and varying total pixel counts. Top; Ø105 μm, NA=0.22, length = 1 m; Middle; Ø200 μm, NA=0.22, length = 1 m; Bottom; Ø200 μm, NA=0.50, length = 1 m.

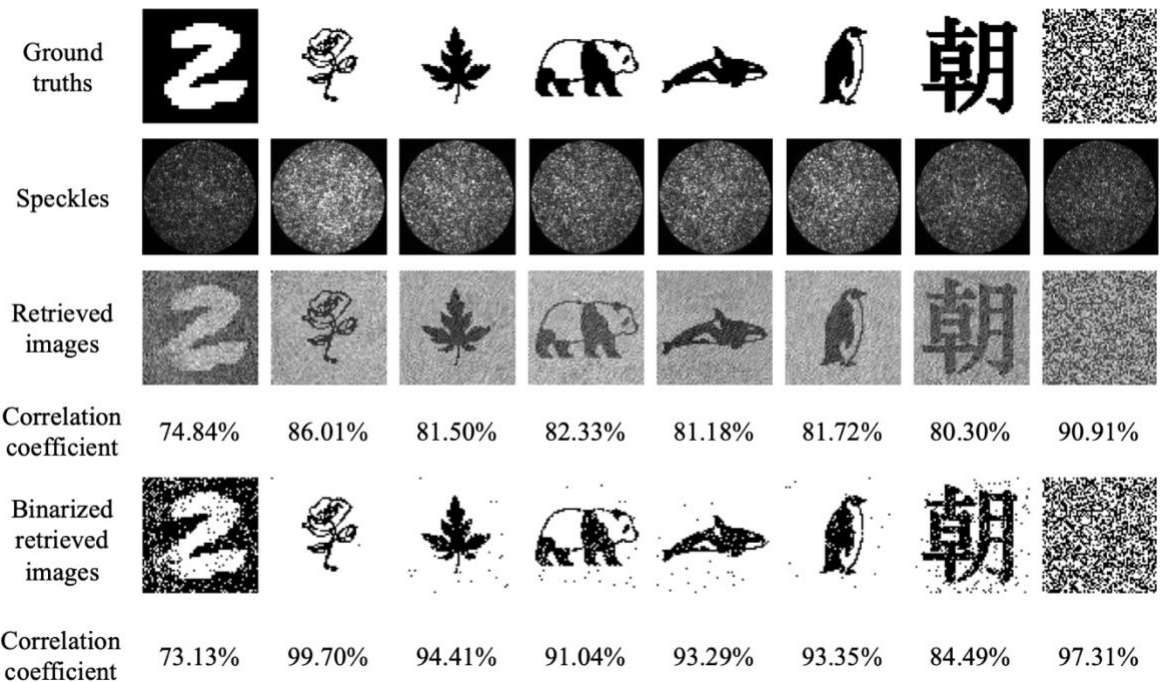


Fig. S2. Some examples of image retrievals through a multimode fiber with different types of input patterns. The pixel count of the ground truths is 64×64 , and the fiber has a core diameter of $200 \mu\text{m}$, a NA of 0.22, and a length of 1 m.

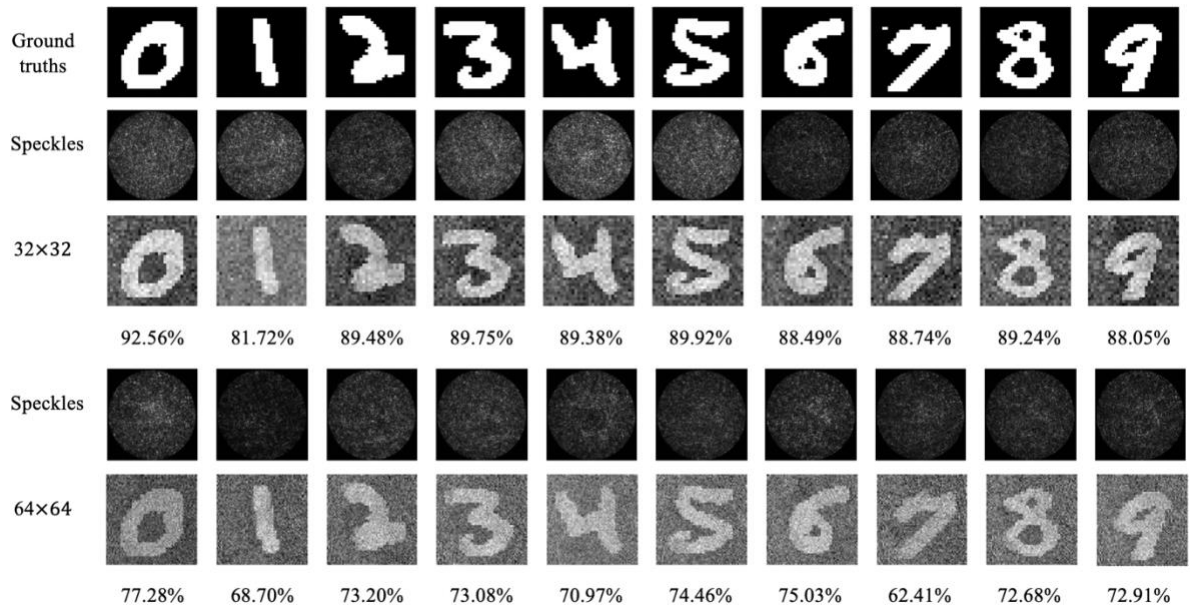


Fig. S3. Some examples of image retrievals through a multimode fiber with handwritten digits with different total pixel counts. The fiber has a core diameter of $200 \mu\text{m}$, a NA of 0.22, and a length of 1 m.

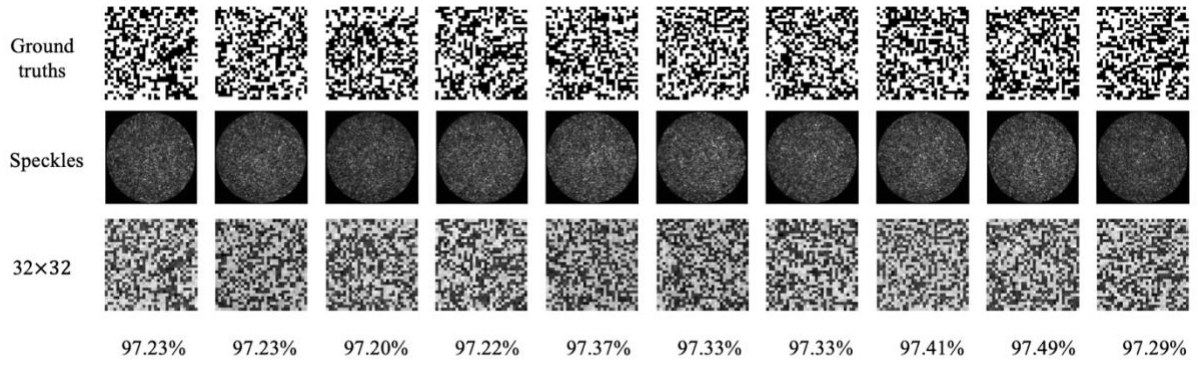


Fig. S4. Some examples of image retrievals through a multimode fiber with 32×32-pixel random patterns. The fiber has a core diameter of 200 μm , a NA of 0.22, and a length of 1 m.

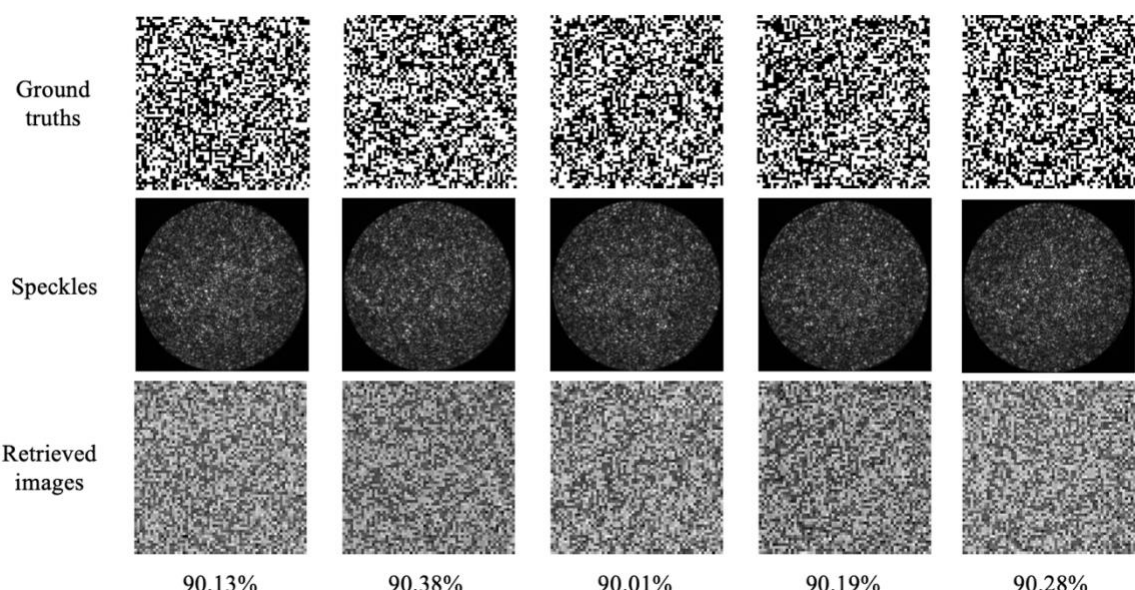
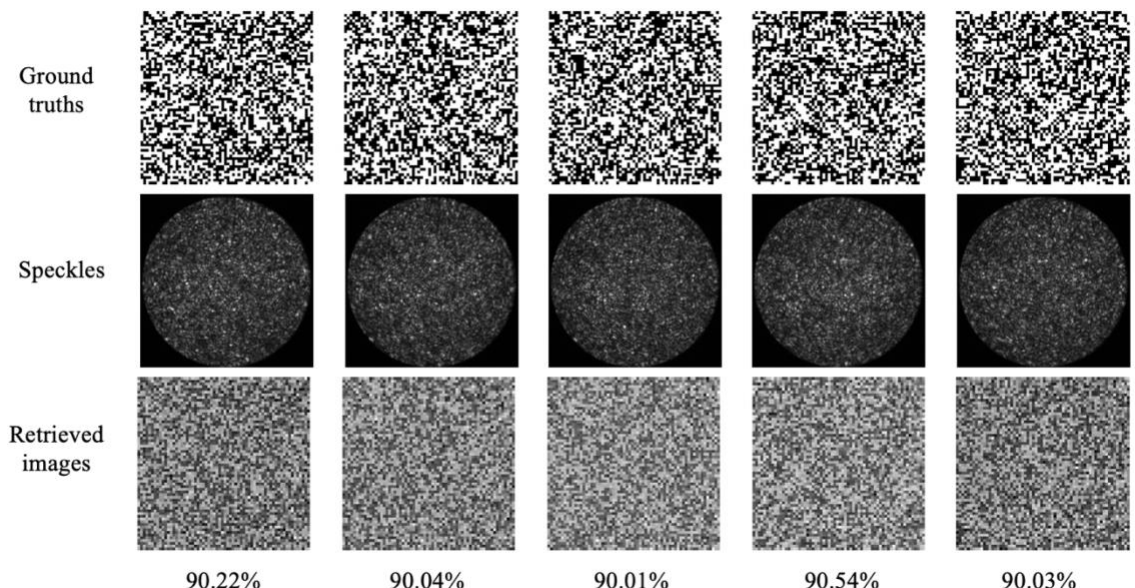


Fig. S5. Some examples of image retrievals through a multimode fiber with 64×64-pixel random patterns. The fiber has a core diameter of 200 μm , a NA of 0.22, and a length of 1 m.

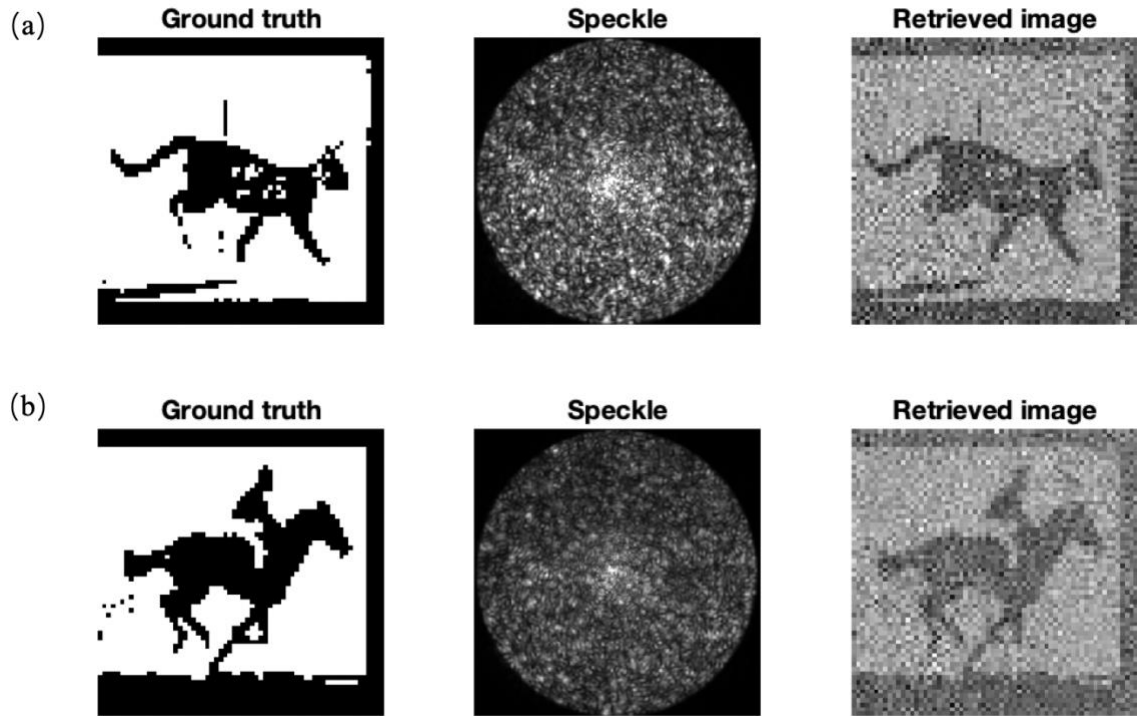


Fig. S6. Examples of individual frames of retrieved videos from the intensity-only output speckles through a multimode fiber with 64×64-pixel random patterns. (a) A moving cat. (b) A man riding a horse. The fiber has a core diameter of 200 μm , a NA of 0.22, and a length of 1 m. The full videos are available in Visualization 1 and Visualization 2. Original images were from the Muybridge collection. Images were binarized for displaying on the DMD.